 doi:10.20944/preprints201708.0037.v1

Lagrangian Meshfree Particle-based Computational Acoustics for Two-dimensional Sound Propagation and Scattering Problems

Yong Ou Zhang[1,2], Xu Li[3], *Tao Zhang[1]

1 School of Naval Architecture and Ocean Engineering, Huazhong University of Science and Technology, Wuhan 430074, China

2 Department of Naval Architecture, Ocean and Structural Engineering, School of Transportation, Wuhan University of Technology, Wuhan 430063, China

3 Wuhan Second Ship Design and Research Institute, Wuhan 430064, China

*Correspondence should be addressed to T. Zhang: zhangt7666@mail.hust.edu.cn

Abstract: Meshfree particle method, which is always regarded as a pure Lagrangian approach, is easily represented complicated domain topologies, moving boundaries, and multiphase media. Solving acoustic problems with the mesfree particle method forms a branch of the acoustic wave modeling field, namely, particle-based computational acoustics (PCA). The aim of this paper is to improve the accuracy of using the PCA method to solve two-dimensional acoustic problems, and realize the particle representation with a hybrid meshfree and finite-difference time-domain (FDTD) method for acoustic boundary conditions at both the plane and curved surface. As a widely used Lagrangian meshfree method, the smoothed particle hydrodynamics (SPH) based on the support domain and the kernel function has developed rapidly in recent years. The traditional SPH method is easily implements parallel processing and has been applied in sound wave simulation. As a corrective method with higher accuracy than SPH, the acoustic propagation and scattering in the time domain is simulated with the corrective smoothed particle method (CSPM). Moreover, a hybrid meshfree-FDTD boundary treatment technique is utilized to represent different acoustic boundaries in the Lagrangian approach. In this boundary treatment technique, the parameter value of virtual particles is obtained with the FDTD method, which concerns truncation errors based on the Tayler series expansion. Soft, rigid, and Mur's absorbing boundary conditions are developed to simulate sound waves in finite and infinite domain. Results of modeling acoustic propagation and scattering show that CSPM is accurate and convergence with exact solutions, and different acoustic boundaries are validated to be effective in the computation.

Keywords: meshfree method; particle-based computational acoustics; smoothed particle hydrodynamics; corrective smoothed particle method; boundary conditions; Lagrangian approach

1. Introduction

Computational acoustic methods have been widely used to simulate the process of sound wave

Preprints (www.preprints.org) | NOT PEER-REVIEWED | Posted: 10 August 2017 doi:10.20944/preprints201708.0037.v1

generation and propagation in complex environments. These numerical methods play a guiding role on the design of structures such as buildings and vehicles, and they become an indispensable part in the optimization of some key components. In the early acoustic computation, the mainly-used methods were two kinds of numerical methods respectively based on boundary discretization with basic theoretical solution and domain-type mesh-based discretization like the boundary element method (BEM) [1, 2], the finite difference method (FDM) [3, 4], the finite element method (FEM) [5, 6], and other modified methods [7, 8]. For the research object with complex geometry, the mesh-based method is more popular due to the unavailability of basic theoretical solutions. However, with this mesh-based method, it is necessary to spend plenty of manpower, material and time resources in the mesh preparation and need the professional quality of users.

In recent years, the meshfree method proposed to solve the above-mentioned problem have attracted much attention in the field of acoustic computation. Since the solution points used in such method are arbitrary in term of spatial distribution, it is unnecessary to spend too much time in the arrangement of solution points even for the research object with complex geometries. Some classic meshfree methods include the method of fundamental solutions (MFS) [9, 10], the reproducing kernel particle method (RKPM) [11, 12], the element-free Galerkin method (EFGM) [13, 14], the equivalent source method (ESM) [15, 16], the singular boundary method (SBM) [17, 18], and other meshfree methods [19, 20].

The present paper focuses on a Lagrangian meshfree particle-based computational acoustic (PCA) method. The PCA method uses the Lagrangian approach, so it is available to simulate the sound generation and propagation from the perspective of fluid particles. It has the following advantages: (i) numerical error accompanying the calculation of advection term is eliminated since the advection term is included in the Lagrangian derivative; (ii) the Lagrangian characteristic makes it easy to handle complex changes of computational domain shape and the problems with moving boundaries; (iii) the interface between different media can be natu

rally tracked by difference in particle density without using any additional algorithm such as the volume of fluid model; (iv) it is available to achieve the derivative solution in a local support domain rather than the entire computational domain so that parallel computing can be easily realized. The introduction of PCA method into acoustic simulation enables these advantages to be fully utilized in the field of computational acoustics, and provides a noval approach for the numerical research of acoustic problems.

Three kinds of governing equations are available to solve problems with PCA methods to date, namely Lagrangian fluid dynamics equations (LFDE), Lagrangian acoustic wave equations (LAWE), and Lagrangian acoustic perturbation equations (LAPE). Among them, LFDE are mainly used for direct numerical simulation (DNS) of sound field, taking the interaction between fluid flow and sound waves into a comprehensive consideration. Based on LFDE, Wolfe [21] simulated the reverberation phenomenon caused by sound generation and reflection inside a room. Hahn [22] used the smoothed

Preprints (www.preprints.org) | NOT PEER-REVIEWED | Posted: 10 August 2017 doi:10.20944/preprints201708.0037.v1

particle hydrodynamics (SPH) method to obtain the pressure disturbance. Zhang et al [23] solved the LFDE with a PCA method, namely the SPH method, to simulate the acoustic propagation in moving media, and the Doppler Effect was solved well. However, because the sound pressure magnitude is much smaller than the pressure magnitude in most engineering problems, for the DNS, a high requirement is imposed on the computational memory and accuracy. The LAWE were established under the assumption of stationary media [24], and it is a special case of LAPE under this assumption. LAWE mainly used for the calculation of far-field acoustic radiation as well as the discussion of computational parameters and acoustic boundaries. In the existing research, the problems on the propagation, reflection, and transmission of sound waves were discussed [25, 26]. LAPE were proposed by Zhang et al [27, 28] based on the acoustic perturbation theory, and the effects of fluid flow on sound waves was considered, so LAPE was supposed to be used as a near-field acoustic source model. Meanwhile, due to the separation of the acoustic propagation process from the flow field solution process, the requirement of this model on computational resources was substantially reduced when compared with DNS. Zhang et al [28] calculated and verified the LAPE with simulating acoustic propagation in uniform flow and vortex flow.

The SPH method is one of the earliest methods and widely applied to different fields. It was first pioneered independently by Lucy [29] and Gingold and Monaghan [30] to solve astrophysical problems in 1977. Details about the SPH computation can be found in recent reviews [31-34] and Liu and Liu's book [35]. Some great successful applications include coastal engineering, nuclear engineering, ocean engineering, and bioengineering. In the recent PCA research, the SPH method is mainly used to model sound propagation, and evaluate the effects of different computational parameters [24, 36]. However, the accuracy of the SPH method is less than second order, which is unsatisfactory for acoustic computation. At present, many improved versions of the conventional SPH method has been proposed to overcome the low accuracy and the lack of consistency. After using the Taylor series expansion to normalize the kernel function, the corrective smoothed particle method (CSPM) [37, 38] and the modified smoothed particle method (MSPH) [39] are proposed. Both two methods have better accuracy than the conventional SPH method. Other modifications or corrections of the SPH method include the finite particle method [40], the symmetrical smoothed particle hydrodynamics method [41, 42], and the moving least square particle hydrodynamics [43, 44] method. In order to improve the accuracy, the present study focuses on using the CSPM as a PCA method for solving LAWE.

Realization of acoustic boundary is a crucial point in computational acoustics, but the implementation of boundary conditions in the particle-based method is not as straightforward as in the mesh-based numerical method since there are not enough particles in the support domain for calculation at the boundary. Virtual particles have been proposed to implement acoustic boundary conditions, and they are allocated on and outside the boundary. However, the pressure and velocity of virtual particles are difficult defined or computed with high accuracy. Limited implementations include

Preprints (www.preprints.org) | NOT PEER-REVIEWED | Posted: 10 August 2017 doi:10.20944/preprints201708.0037.v1

rigid and soft acoustic boundaries for one-dimensional problems [25, 26]. In the present paper, the finite-difference time-domain (FDTD) method is combined with virtual particles to realize the two-dimensional acoustic boundary condition, which is named as the hybrid meshfree-FDTD method [45]. Different boundary conditions on the flat plane and curved surface are built and tested. This hybrid method is supposed to improve the boundary accuracy with high order Taylor series expansion in the finite difference scheme.

The present paper is organized as follows. In Section 2, SPH and CSPM formulations for acoustic waves are given. In Section 3, hybrid mesfree-FDTD method for acoustic boundary treatment is introduced. In Section 4 and 5, applications of particle methods to sound propagation and scattering problems are tested separately. Section 6 summarizes the results of this work.

2. SPH and CSPM formulations for acoustic waves

2.1 Basic concepts of SPH

The concept of integral representation for $f(\boldsymbol{r})$ used in the SPH method can be written as a particle approximation form

$$< f(\boldsymbol{r}) >= \int_{\Omega} f(\boldsymbol{r}')W(\boldsymbol{r}-\boldsymbol{r}',h)\,\mathrm{d}\boldsymbol{r}' \tag{1}$$

where f is a function of the position vector $\boldsymbol{r}$, W is the smoothing kernel function, h is the smoothing length defines the influence area of the smoothing function.

The kernel approximation of $f(\boldsymbol{r})$ and $\nabla\cdot f(\boldsymbol{r})$ used in the SPH method can be described as a summation of neighboring particles as

$$< f(\boldsymbol{r}) >= \sum_{j=1}^{N} \frac{m_j}{\rho_j} f(\boldsymbol{r}_j)W_{ij} \tag{2}$$

$$< \nabla\cdot f(\boldsymbol{r}) >= -\sum_{j=1}^{N} \frac{m_j}{\rho_j} f(\boldsymbol{r}_j)\cdot\nabla_i W_{ij} \tag{3}$$

where $W_{ij}=W(\boldsymbol{r}-\boldsymbol{r}_j,h)$, N indicates the number of particles in the support domain, m_j is the mass of particle j, and ρ_j is the density of particle j. In the SPH convention, the kernel approximation operator is marked by the angle bracket <>.

Present paper uses the cubic spline kernel function as the smoothing kernel function. The cubic spline kernel is a widely used smoothing function which was originally used by Monaghan and Lattanzio [46].

2.2 SPH formulations for acoustic waves

2.2.1 Lagrangian acoustic wave equations

In fluid dynamics, the Lagrangian form governing equations for constructing SPH formulations

Preprints (www.preprints.org) | NOT PEER-REVIEWED | Posted: 10 August 2017 doi:10.20944/preprints201708.0037.v1

are the laws of continuity, momentum and state which can be found in Chapter 4 of [35]. For most common acoustical problems, there are two assumptions are always used to simplify the question. On one hand, the medium is lossless and at rest. On the other hand, a small departure from quiet conditions occurs. In this work, the medium for sound propagation and reflection is ideal fluid, and the process is adiabatic. In addition, sound pressure δp, the density change of particle $\delta\rho$ and the particle velocity $\delta\boldsymbol{v}$ are supposed small, which can be expressed as

$$\begin{cases} P = p_0 + \delta p, & |\delta p| << p_0 \\ \rho = \rho_0 + \delta\rho, & |\delta\rho| << \rho_0 \\ \boldsymbol{v} = \boldsymbol{v}_0 + \delta\boldsymbol{v}, & |\delta\boldsymbol{v}| << c_0 \end{cases} \tag{4}$$

where ρ is the fluid density, $\boldsymbol{v}$ is the flow velocity, P is the pressure and c_0 is the speed of sound.

Substitute these expressions into the continuity and momentum equations and considering ρ_0 and p_0 remains the same during the computation. To evaluate the acoustic boundary condition, we use LAWE for modeling sound waves in stationary media. Ignoring $\boldsymbol{v}_0$ and small quantities of first order, the continuity and momentum equations governing sound waves can be written as

$$\frac{\mathrm{D}\delta\rho}{\mathrm{D}t} = -\rho_0 \nabla \cdot \delta\boldsymbol{v} \tag{5}$$

$$\frac{\mathrm{D}\delta\boldsymbol{v}}{\mathrm{D}t} = -\frac{1}{\rho_0}\nabla\delta p \tag{6}$$

The state equation for ideal gas is written as

$$\frac{\mathrm{D}\delta p}{\mathrm{D}t} = c_0^2 \frac{\mathrm{D}\delta\rho}{\mathrm{D}t} \tag{7}$$

2.2.2 particle approximation of governing equations

Applying the particle approximation equation (Eq. (3)) to the continuity equation (Eq. (5)) and adding the gradient of the unity [35], SPH formulation for the continuity equation can be obtained as

$$\frac{\mathrm{D}\delta\rho_i}{\mathrm{D}t} = -(\rho_0 + \delta\rho_i)\sum_{j=1}^{N}\frac{m_j}{(\rho_0 + \delta\rho_j)}\delta\boldsymbol{v}_{ij}\nabla_i W_{ij} \tag{8}$$

where the subscript i and j stand for variables associated with particles i and j, $\delta\boldsymbol{v}_{ij} = \delta\boldsymbol{v}_i - \delta\boldsymbol{v}_j$. Considering Eq. (4), the continuity equation can be written as

$$\frac{\mathrm{D}\delta\rho_i}{\mathrm{D}t} = -\sum_{j=1}^{N} m_j \delta\boldsymbol{v}_{ij}\nabla_i W_{ij} \tag{9}$$

Applying the particle approximation equation (Eq. (3)) to the momentum equation (Eq. (6)), it appears as

$$\frac{\mathrm{D}\delta\boldsymbol{v}_i}{\mathrm{D}t} = -\frac{1}{(\rho_0 + \delta\rho_i)}\sum_{j=1}^{N}\frac{m_j}{(\rho_0 + \delta\rho_j)}\delta p_j \nabla_i W_{ij} \tag{10}$$

Other forms of the momentum equation can be written as

Preprints (www.preprints.org) | NOT PEER-REVIEWED | Posted: 10 August 2017 doi:10.20944/preprints201708.0037.v1

$$\frac{\mathrm{D}\delta \boldsymbol{v}_i}{\mathrm{D}t} = -\sum_{j=1}^{N} m_j \frac{\delta p_i + \delta p_j}{(\rho_0 + \delta\rho_i)(\rho_0 + \delta\rho_j)} \nabla_i W_{ij} \tag{11}$$

$$\frac{\mathrm{D}\delta \boldsymbol{v}_i}{\mathrm{D}t} = -\sum_{j=1}^{N} m_j \left[\frac{\delta p_i}{(\rho_0 + \delta\rho_i)^2} + \frac{\delta p_j}{(\rho_0 + \delta\rho_j)^2} \right] \nabla_i W_{ij} \tag{12}$$

Particle approximation of the equation of state for ideal gas is

$$\frac{\mathrm{D}\delta p_i}{\mathrm{D}t} = c_0^2 \frac{\mathrm{D}\delta\rho_i}{\mathrm{D}t} \tag{13}$$

2.3 CSPM formulations for acoustic waves

The Taylor series expansion is used to improve the accuracy of the SPH method, which is named as CSPM [37, 38]. If a function $f(\boldsymbol{x})$ is assumed to be sufficiently smooth in a domain that contains $\boldsymbol{x}$, the Taylor series expansion for $f(\boldsymbol{x}_j)$ in the vicinity of $\boldsymbol{x}_i$ can be written as

$$f(\boldsymbol{x}_j) = f(\boldsymbol{x}_i) + (\boldsymbol{x}_j^{\alpha} - \boldsymbol{x}_i^{\alpha}) f_{\alpha}(\boldsymbol{x}_i) + \frac{1}{2!}(\boldsymbol{x}_j^{\alpha} - \boldsymbol{x}_i^{\alpha})(\boldsymbol{x}_j^{\beta} - \boldsymbol{x}_i^{\beta}) f_{\alpha\beta}(\boldsymbol{x}_i) + \ldots \tag{14}$$

where $\alpha, \beta = 1, 2, 3$, represent different dimensional space.

In the local support domain Ω of $\boldsymbol{x}$, multiplying both sides of Equation (14) with a smoothing kernel function $W(\boldsymbol{x}_j - \boldsymbol{x}_i, r_e)$ of compact circular support of radius r_e, and integrating over the support domain, the following formulation can be obtained

$$\begin{aligned} \int_{\Omega} f(\boldsymbol{x}_j) W \, \mathrm{d}\boldsymbol{x}_j = & \int_{\Omega} f(\boldsymbol{x}_i) W \, \mathrm{d}\boldsymbol{x}_j + \int_{\Omega} (\boldsymbol{x}_j^{\alpha} - \boldsymbol{x}_i^{\alpha}) f_{\alpha}(\boldsymbol{x}_i) W \, \mathrm{d}\boldsymbol{x}_j \\ & + \int_{\Omega} \frac{1}{2!} (\boldsymbol{x}_j^{\alpha} - \boldsymbol{x}_i^{\alpha})(\boldsymbol{x}_j^{\beta} - \boldsymbol{x}_i^{\beta}) f_{\alpha\beta}(\boldsymbol{x}_i) W \, \mathrm{d}\boldsymbol{x}_j + \ldots \end{aligned} \tag{15}$$

From the above equation, a corrective kernel approximation for function $f(\boldsymbol{x})$ at $\boldsymbol{x}_i$ can be written as

$$< f(\boldsymbol{x}_i) >= \frac{\int_{\Omega} f(\boldsymbol{x}_j) W \, \mathrm{d}\boldsymbol{x}_j}{\int_{\Omega} W \, \mathrm{d}\boldsymbol{x}_j} \tag{16}$$

Replacing $W(\boldsymbol{x}_j - \boldsymbol{x}_i, r_e)$ with $\nabla W(\boldsymbol{x}_j - \boldsymbol{x}_i, r_e)$, a corrective kernel approximation for the first derivative of $f(\boldsymbol{x})$ at $\boldsymbol{x}_i$ can be written as

$$f_{\alpha}(\boldsymbol{x}_i) = \frac{\int_{\Omega} f(\boldsymbol{x}_j) \nabla W \, \mathrm{d}\boldsymbol{x}_j - \int_{\Omega} f(\boldsymbol{x}_i) \nabla W \, \mathrm{d}\boldsymbol{x}_j}{\int_{\Omega} (\boldsymbol{x}_j^{\alpha} - \boldsymbol{x}_i^{\alpha}) \nabla W \, \mathrm{d}\boldsymbol{x}_j} \tag{17}$$

The particle formulations of Equations (16) and (17) are given as

Preprints (www.preprints.org) | NOT PEER-REVIEWED | Posted: 10 August 2017 doi:10.20944/preprints201708.0037.v1

$$f(\boldsymbol{x}_i)=\frac{\sum_{j=1}^{N}\frac{m_j}{\rho_j}f(\boldsymbol{x}_j)W_{ij}}{\sum_{j=1}^{N}\frac{m_j}{\rho_j}W_{ij}} \tag{18}$$

$$f_\alpha(\boldsymbol{x}_i)=\frac{\sum_{j=1}^{N}\frac{m_j}{\rho_j}\left[f(\boldsymbol{x}_j)-f(\boldsymbol{x}_i)\right]\nabla_i W_{ij}}{\sum_{j=1}^{N}\frac{m_j}{\rho_j}(\boldsymbol{x}_j^\alpha-\boldsymbol{x}_i^\alpha)\nabla_i W_{ij}} \tag{19}$$

The second order leap-frog integration is used in the paper to update parameters, and all-pair searching approach is used to realize the neighbour particle searching. The code is developed from a one-dimensional SPH algorithm used in [45].

3. Hybrid meshfree-FDTD method for acoustic boundary treatment

3.1 Hybrid meshfree-FDTD method

Meshfree method suffers from the problem that not enough particles in the support domain can be used for the CSPM computation. In the present paper, the FDTD method is introduced to combine with the virtual particle technique, and thus a technique based on the meshfree-FDTD hybrid method for acoustic boundary treatment is accordingly constructed. The feasibility and validity of the meshfree-FDTD hybrid method is verified by simulating sound propagation in pipes with boundaries.

Since the FDTD method is proposed by Yee [47] in 1966, it has received widely concern, and used to solve problems in many different research fields. The FDTD method can solve fundamental equations in the time domain. In this paper, for building the meshfree-FDTD hybrid method, the FDTD method proposed by Wang [48] that used to simulate underwater acoustic boundary and the virtual particle technique are combined.

In the hybrid meshfree-FDTD boundary treatment, three types of particles need to be built before computation, namely the fluid particle, the boundary particle, and the virtual particle. During the computation, the numerical method for these three kinds of particles are shown as below

$$\text{boundary treatment for particle } i = \begin{cases} \text{meshfree method (SPH/CSPM)} & \text{if } i=\text{fluid particles} \\ \text{meshfree method (SPH/CSPM)} & \text{if } i=\text{boundary particles} \\ \text{FDTD method} & \text{if } i=\text{virtual particles} \end{cases}$$

The meshfree method like the SPH and CSPM method is used for fluid particles and boundary particles, and the FDTD method is used for virtual particles.

3.2 Boundary conditions on plane

On a boundary, virtual particles can be obtained through extending boundary particles to the

Preprints (www.preprints.org) | NOT PEER-REVIEWED | Posted: 10 August 2017 doi:10.20944/preprints201708.0037.v1

outside of the computation region, and the distribution of virtual particles are regular, the number of layer can be chosen according to the scale of support domain. Figure 1 is the sketch of the treatment of particles near the wall. i represents the particle number and Δx is the particle spacing.

In the present work, the CSPM is used for computing boundary particles and fluid particles, and virtual particles are computed through the FDTD method, so it can be named as a hybrid CSPM-FDTD method for the boundary treatment. Some simple forms for representing virtual particles are obtained in this section. Other high order forms for virtual particles can also be derived by users with high order finite difference schemes.

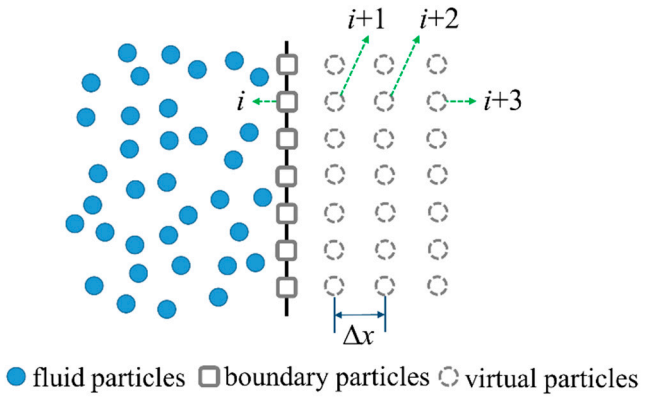

Figure 1. The sketch of simulating acoustic boundary by using hybrid CSPM-FDTD method.

For the rigid case, acoustic boundary conditions are

$$\frac{\partial \delta p}{\partial \boldsymbol{n}} = 0,\ \delta \boldsymbol{v} = 0 \tag{20}$$

where $\boldsymbol{n}$ represents the normal direction of surface. Assuming the initial particle spacing is Δx, according to the first order FDTD scheme we have

$$\frac{\delta p_{i+1} - \delta p_i}{\Delta x} = 0,\ \delta \boldsymbol{v}_{i+1} = 0 \tag{21}$$

which can be written as

$$\delta p_{i+1} = \delta p_i,\ \delta \boldsymbol{v}_{i+1} = 0 \tag{22}$$

In the same way, the particle-based boundary conditions for rigid case become

$$\delta p_{i+3} = \delta p_{i+2} = \delta p_{i+1} = \delta p_i,\ \delta \boldsymbol{v}_{i+3} = \delta \boldsymbol{v}_{i+2} = \delta \boldsymbol{v}_{i+1} = 0 \tag{23}$$

For the soft boundary, sound pressure satisfices the following:

$$\delta p = 0 \tag{24}$$

The formulation for virtual particles is written as

$$\delta p_{i+1} = \delta p_{i+2} = \delta p_{i+3} = 0 \tag{25}$$

According to the finite difference scheme, the velocity of virtual particles on the first layer (e.g. particle i+1) should be calculated from the momentum equation as

Preprints (www.preprints.org) | NOT PEER-REVIEWED | Posted: 10 August 2017 doi:10.20944/preprints201708.0037.v1

$$\frac{\delta u_{i+1}^{(n)} - \delta u_{i+1}^{(n-1)}}{\Delta t} = -\frac{1}{\rho_0}\frac{\delta p_{i+2}^{(n-1)} - \delta p_i^{(n-1)}}{2\Delta x}, \delta v_{i+1}^{(n)} = 0 \tag{26}$$

which can be written as

$$\delta u_{i+1}^{(n)} = \delta u_{i+1}^{(n-1)} + \frac{\delta p_i^{(n-1)}\Delta t}{2\rho_0 \Delta x}, \delta v_{i+1}^{(n)} = 0 \tag{27}$$

where superscript n represents the temporal index, δu is the normal velocity on the surface, and δv is the parallel velocity on the surface.

For other virtual particles from the second to the last layer, the velocity boundary condition at any time are written as

$$\delta u_{i+2} = \delta u_{i+3} = 0, \delta v_{i+2} = \delta v_{i+3} = 0 \tag{28}$$

For the absorbing boundary condition, the popular first-order absorbing boundary condition (ABC) proposed by Mur is used in the present work. Assuming that the ABC is located at $x = x_1$, sound propagates from the right side to the left side. The ABC can be written as

$$\left[\frac{\partial f}{\partial x} - \frac{1}{c_0}\frac{\partial f}{\partial t}\right]_{x=x_1} = 0 \tag{29}$$

where the field parameter f can be δp, δu or δv in this equation. This leads to a difference expression for virtual particles used in the meshfree-FDTD hybrid method, and the particle-based boundary conditions become

$$f_{i+1}^{(n)} = f_i^{(n-1)} + \frac{c_0\Delta t - \Delta x}{c_0\Delta t + \Delta x}(f_i^{(n)} - f_{i+1}^{(n-1)}) \tag{30}$$

$$f_{i+2}^{(n)} = f_i^{(n-1)} + \frac{c_0\Delta t - 2\Delta x}{c_0\Delta t + 2\Delta x}(f_i^{(n)} - f_{i+2}^{(n-1)}) \tag{31}$$

$$f_{i+3}^{(n)} = f_i^{(n-1)} + \frac{c_0\Delta t - 3\Delta x}{c_0\Delta t + 3\Delta x}(f_i^{(n)} - f_{i+3}^{(n-1)}) \tag{32}$$

The field parameter f in this equation are δp, δu, or δv.

Preprints (www.preprints.org) | NOT PEER-REVIEWED | Posted: 10 August 2017 doi:10.20944/preprints201708.0037.v1

3.3 Boundary conditions on curved surface

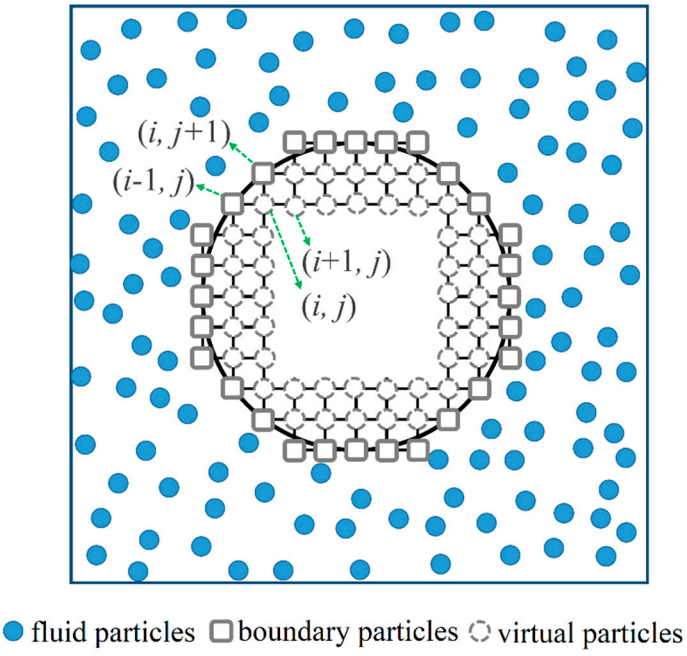

Figure 2. The sketch of simulating acoustic boundary on curved surface by by using the hybrid meshfree-FDTD method with type II particle distribution.

The curved surface is another widely used geometry for engineering problems, and the combination of flat and curved surface generates variety of shapes for different objects. So the acoustic boundary on two-dimensional curved surface is realized with the hybrid meshfree-FDTD method in this section.

Two different particle distribution types are introduced, and the type I distribution is shown in Figure 2. Virtual particles are uniformly distributed inside the object with initial particle spacing Δx. For the rigid boundary, sound pressure satisfies the following:

$$\frac{\partial \delta p}{\partial x}\cos\alpha+\frac{\partial \delta p}{\partial y}\sin\alpha=0 \tag{33}$$

where α is the angle between the surface normal and the horizontal axis. Assuming virtual particles (i, j), (i, j+1), and (i-1, j) are as shown in Fig. 2, the following relation can be obtained

$$\delta p_{i,j}^{(n)}=\frac{-\delta p_{i-1,j}^{(n)}\cos\alpha+\delta p_{i,j+1}^{(n)}\sin\alpha}{-\cos\alpha+\sin\alpha} \tag{34}$$

For the two components of $\delta \boldsymbol{v}$, δu and δv, one can be calculated from the recurrence relation, using biased rather than central difference as

$$\frac{\delta u_{i,j}^{(n)}-\delta u_{i,j}^{(n-1)}}{\Delta t}=-\frac{1}{\rho_0}\frac{\delta p_{i,j}^{(n-1)}-\delta p_{i-1,j}^{(n-1)}}{\Delta x} \tag{35}$$

which can be written as

Preprints (www.preprints.org) | NOT PEER-REVIEWED | Posted: 10 August 2017 doi:10.20944/preprints201708.0037.v1

$$\delta u_{i,j}^{(n)} = \delta u_{i,j}^{(n-1)} - \frac{\Delta t}{\rho_0 \Delta x}(\delta p_{i,j}^{(n-1)} - \delta p_{i-1,j}^{(n-1)}) \tag{36}$$

The other should be calculated from the following relation:

$$\delta v_{i,j}^{(n)} \sin\alpha = -\delta u_{i,j}^{(n)} \cos\alpha \tag{37}$$

Type II distribution is shown in Figure 3. Virtual particles are set along the radial distribution inside the object.

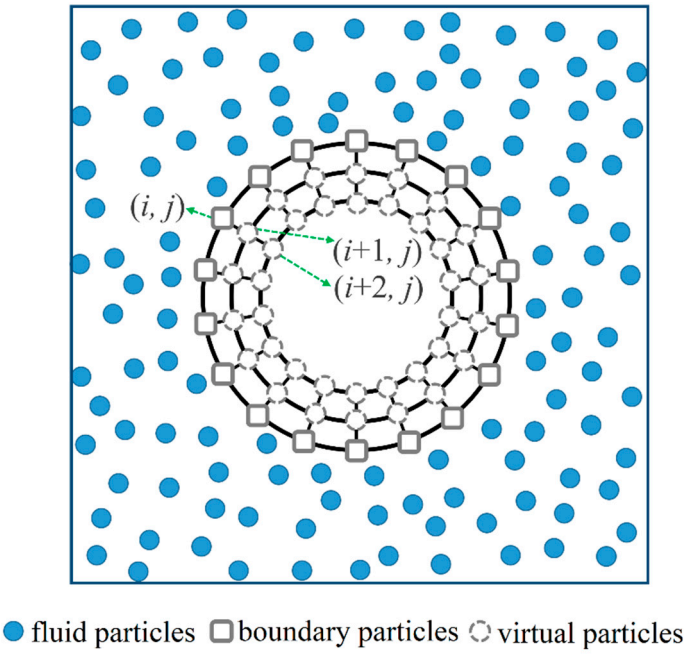

Figure 3. The sketch of simulating acoustic boundary on curved surface by using the hybrid meshfree-FDTD method with type I particle distribution.

For the rigid boundary, the particle-based boundary conditions are derived from Eq. (20) as

$$\delta p_{i+2,j} = \delta p_{i+1,j} = \delta p_{i,j},\ \delta \boldsymbol{v}_{i+2,j} = \delta \boldsymbol{v}_{i+1,j} = 0 \tag{38}$$

4. Sound propagation simulation with CSPM

4.1 Sound propagation model

Sound propagation along ducts is computed to evaluate the CSPM algorithm. In this model, sound propagates along the x-axis. The CSPM computational domain is from -50 m to 150 m, and the computation time is 1.25 s.

Sound pressure of the acoustic source wave is written as

$$\delta p(t, x < 0) = P_{\mathrm{A}} \sin(\omega t - kx) \tag{39}$$

where t denotes time, x is the geometric position in the propagation direction, ω is the angular

Preprints (www.preprints.org) | NOT PEER-REVIEWED | Posted: 10 August 2017 doi:10.20944/preprints201708.0037.v1

frequency of the sound wave, $k = \omega / c_0$ is the wave number. Sound speed c_0= 340 m/s and ω= 340 rad/s. The Courant-Friedriches-Lewy number is written as C_{CFL} for short, and $C_{CFL} = u\Delta t / \Delta x$.

4.2 Validation and discussion of the PCA method

Based on the sound propagation model and computational parameters, the CSPM algorithms is built to solve acoustic wave equations. Then, the CSPM simulation results are compared to theoretical solutions as shown in Figure 3. In this figure, solid lines demonstrate theoretical solutions, and black scattered points represent the CSPM simulation results. For clearly identifying the SPH results, the scattered points are plotted at intervals of 14 grid points.

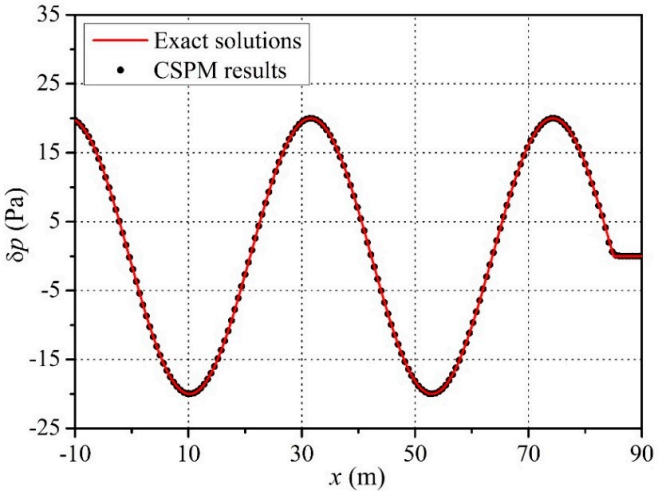

Figure 4. Sound pressure computation between CSPM results and theoretical solutions.

From the figure, it can be seen that the CSPM simulation results agree well with theoretical solutions. Several peaks and valleys appear in the graph between -50 m and 150 m, and sound pressure amplitudes of the computational case agree well with each other. In general, CSPM simulation results is stable.

Numerical accuracy of the present CSPM method is discussed. The method is compared with theoretical solutions. The numerical accuracy is calculated by the relative root mean square errors (L_{error}) and the maximum error (M_{error}), which are given as follows:

$$L_{err}(\delta p) = \frac{\sqrt{\frac{1}{N}\sum_{i=1}^{N}\left|\delta p_i - \delta \overline{p}_i\right|^2}}{\sqrt{\frac{1}{N}\sum_{i=1}^{N}\left|\delta \overline{p}_i\right|^2}} \tag{40}$$

$$M_{err}(\delta p) = \max_{1\le i\le N}\left|\delta p_i - \delta \overline{p}_i\right| \tag{41}$$

where δp_i and $\delta \overline{p}_i$ are simulation results and theoretical solutions at particle i, and N is the total number of particles in the computation domain.

Sound propagation using the CSPM algorithm with particle spacing changing from 0.02 to 0.10

Preprints (www.preprints.org) | NOT PEER-REVIEWED | Posted: 10 August 2017 doi:10.20944/preprints201708.0037.v1

m is computed. Then, we calculate the CSPM numerical error of sound pressure according to Eq. (40) and (41), as shown in Figure 5.

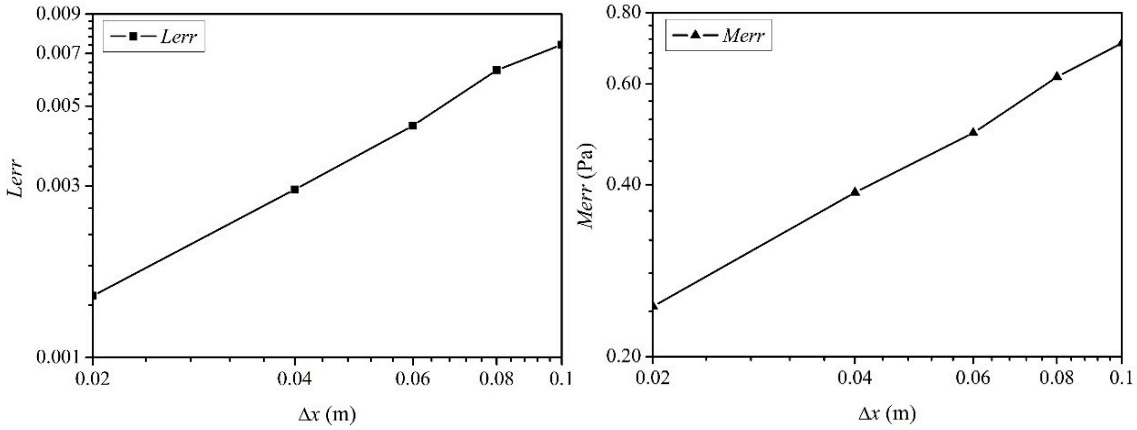

Figure 5. Convergence curve for the CSPM method.

From the figure, it can be seen that, with the increasing of particle spacing, L_{error} and M_{error} increase gradually. L_{error} and M_{error} are the smallest at particle spacing Δx = 0.02 m, which are 1.5×10^{-3} and 0.047 Pa, respectively. When particle spacing Δx = 0.10 m, L_{error} and M_{error} are 0.126 and 1.17 Pa, respectively. In conclusion, the CSPM algorithm shows a good convergence in the simulation of sound propagation.

Similarly, numerical error of sound propagation by using the CSPM algorithms with different C_{CFL} is also discussed. When C_{CFL} changes from 0.05 to 0.32, L_{error} and M_{error} are computed as shown in Figure 6.

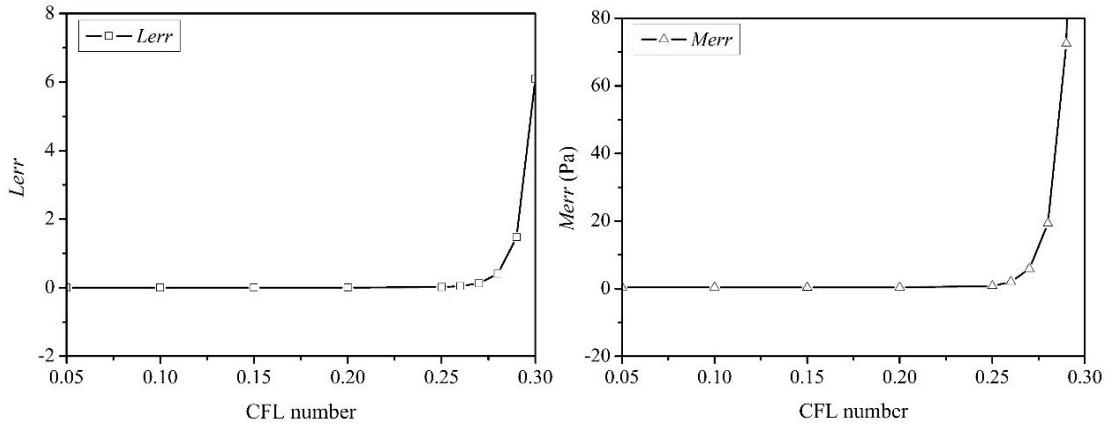

Figure 6. Sound pressure error versus C_{CFL} in the CSPM computation.

As can be seen from the figure, in the region of $0.05\leq C_{CFL}\leq 0.28$, with the increasing of C_{CFL}, L_{error} and M_{error} increase slowly. When C_{CFL} equals to 0.05, L_{error} and M_{error} are 0.02 and 0.19 Pa, respectively. While C_{CFL} is 0.28, L_{error} and M_{error} are 0.03 and 0.20 Pa. Moreover, when C_{CFL} is greater than 0.28, L_{error} and M_{error} increase sharply with increased C_{CFL}. In general, for maintaining the computational accuracy and efficiency in the numerical simulation, C_{CFL} is preferably set as under 0.28.

Preprints (www.preprints.org) | NOT PEER-REVIEWED | Posted: 10 August 2017 doi:10.20944/preprints201708.0037.v1

5. Acoustic boundary application

5.1 Sound propagation of Gaussian pulse

To validate the feasibility and accuracy of two-dimensional sound propagation by using the CSPM codes. A Guassian pulse model of sound propagation is built, as shown in Figure 6. This model is similarly to the model given by ICASE/LaRC workshop, which are proposed for solving the benchmark problem in computational aeroacoustics (CAA). Figure 7 (a) gives the contour of sound pressure at t = 0 s. The center of computation region is located at the origin of coordinates, the computation domain is a square, and the length of square is 100 m. Figure 7 (b) is the changing trend of sound pressure at y = 0 m.

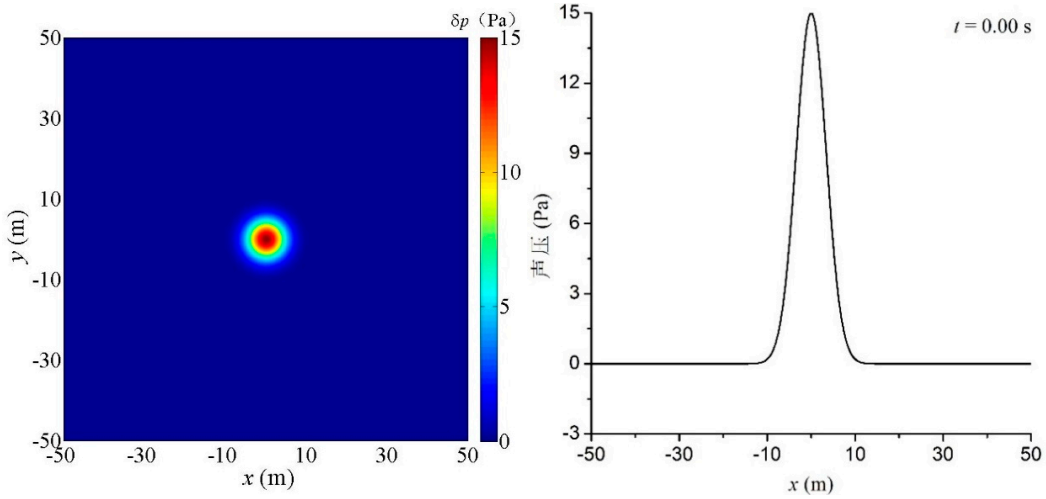

(a) (b)

Figure 7. The initial sound pressure of Guassian pulse.

At the time t = 0 s, the distribution of the sound pressure of Guassian pulse model in the computation domain can be written as

$$\delta p(t=0, x, y) = \alpha_1 \rho_0 c_0^2 \exp\left[-\alpha_2 \left(x^2 + y^2\right)\right] \tag{42}$$

where α_1 =15 / c_0^2， α_2 =ln 2 / 16， c_0 = 340 m / s, ρ_0 is the initial density of medium, x represents the horizontal coordinates of the particle in the computation domain, while y represents the vertical coordinate of the particle.

The theoretical solution of the sound pressure of Guassian pulse can be written as the follow form

$$\delta p(t, x, y) = \frac{\alpha_1 \rho_0 c_0^2}{2\alpha_2} \int_0^\infty \exp\left(\frac{-\xi^2}{4\alpha_2}\right) \cos(\xi t) J_0(\xi \eta) \xi d\xi \tag{43}$$

where ξ is the integral operator, $\eta = \sqrt{x^2 + y^2}$, J_0 represents the zero order Bessel function.

On the basis of the Guassian pulse of sound propagation, Table 1 lists the computational parameters that are used in the simulation of the Guassian pulse of sound propagation.

Preprints (www.preprints.org) | NOT PEER-REVIEWED | Posted: 10 August 2017 doi:10.20944/preprints201708.0037.v1

Table 1. Parameters for the CSPM algorithms of sound propagation of the Guassian pulse.

Computational parameters	Values
Particle spacing Δx, Δy	0.20 m, 0.20 m
h	0.22 m
Kernel type	cubic spline
C_{CFL}	0.20
c_0	340 m/s
ρ_0	1.0 kg/m^3

The simulation results of the Guassian pulse of sound propagation are shown in Figure 8. Figure 8 (a), (b) gives the contour of sound pressure at t = 0.05 s and 0.10 s. It can be seen that the acoustic wave propagates to all around in the form of circle, and the center of circle is located at the origin of the coordinate. The speed of propagation is 340 m/s. As time goes on, the radius of the circle increases, while the amplitude of the sound waves decreases.

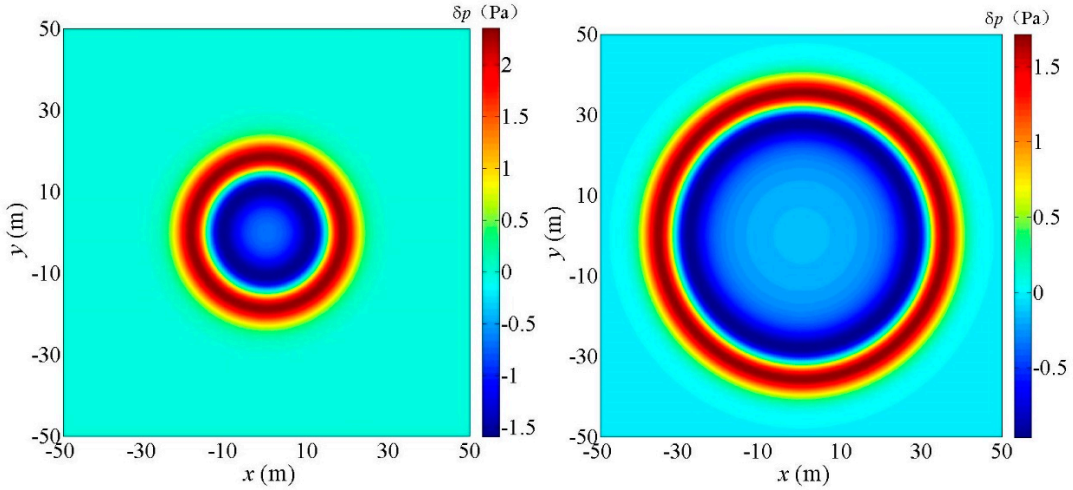

(a) t= 0.05 s (b) t = 0.10 s

Figure 8. The sound pressure contour of sound propagation at different time.

For providing a better comparison, the sound pressure of particles at y = 0 m are extracted, and compared with the theoretical solution, as shown in Figure 9. In the figure, the red solid line represents the theoretical solution, the black scattered points represents the simulation results at y = 0 m.

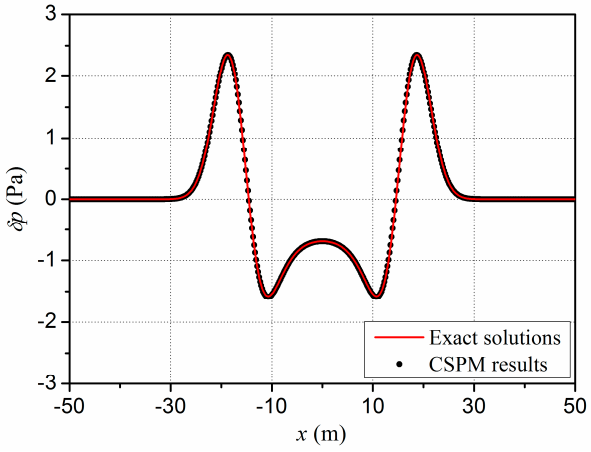

Figure 9. The sound pressure of particles at x-axis.

Preprints (www.preprints.org) | NOT PEER-REVIEWED | Posted: 10 August 2017 doi:10.20944/preprints201708.0037.v1

From the figure, it can be seen that, at y = 0 m, the CSPM simulation results possess similar smoothing trends compared to the theoretical solution. With the time increasing, the amplitude of the peaks and valleys decreases. Generally, the CSPM algorithms and codes can simulate the Guassian pulse of sound propagation well.

5.2 Soft boundary

The sound propagation model with soft boundary is built to validate the accuracy of the hybrid CSPM-FDTD method. The computation domain is -50 m $\le x \le$ 50 m and -50 m $\le y \le$ 50 m. The soft boundary is located at x = ±50 m and y = ±50 m. At the time t = 0 s, the distribution of the sound pressure of Guassian pulse model in the computation domain is written as

$$\delta p\left(t=0, x, y\right)=\alpha_1 \rho_0 c_0^2 \exp\left\{-\alpha_2\left[(x-12.5)^2+y^2\right]\right\} \tag{44}$$

where α_1 =15 / c_0^2， α_2 =ln 2/16， c_0 = 340 m / s. Then, Sound pressure at t = 0 s, 0.05 s, 0.10 s, 0.15 s are computed, the simulation results are shown in Figure 10.

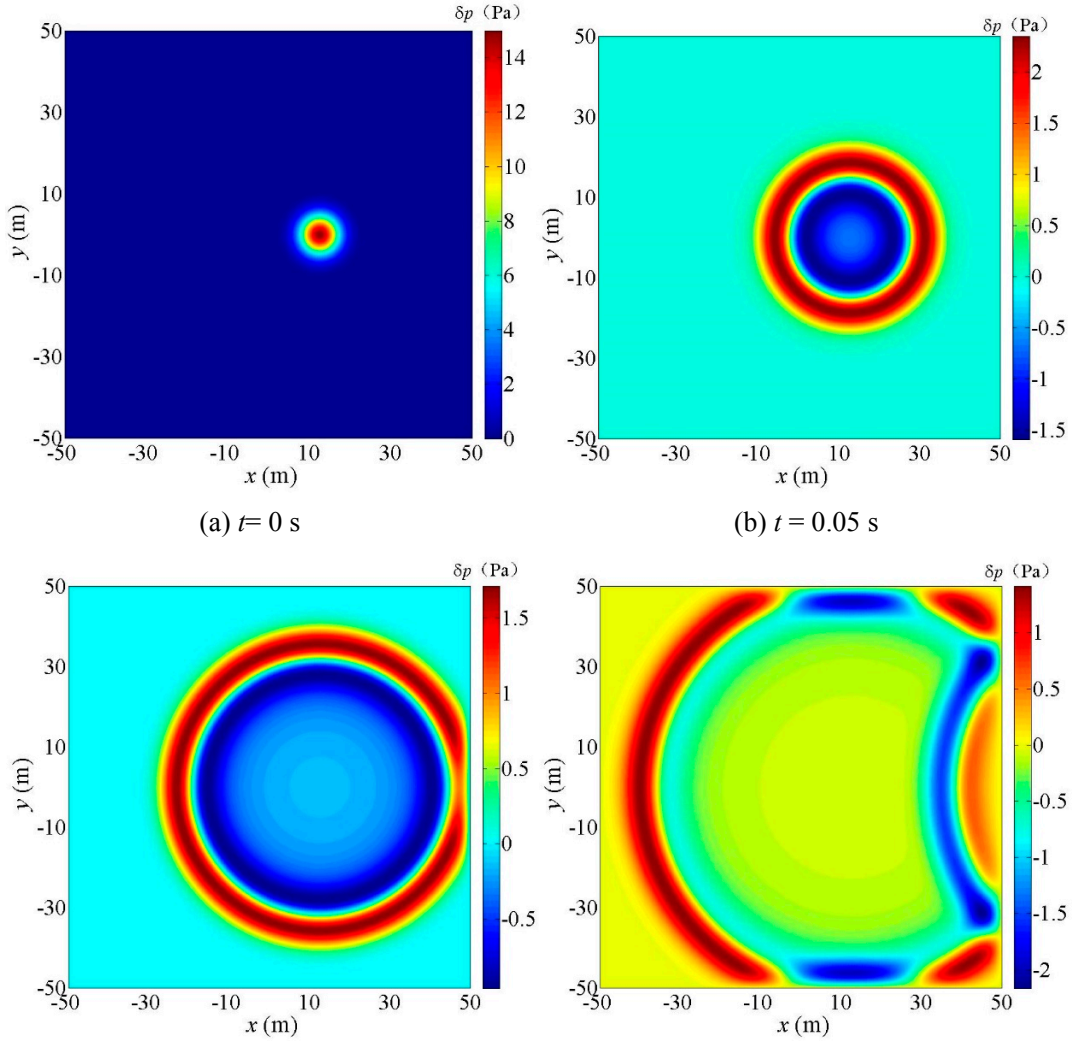

Figure 10. Sound pressure contour of the Guassian pulse under the effect of soft boundary.

Figure 10(a) shows the sound pressure at initial time. Figure 10(b) is the sound pressure at t =

Preprints (www.preprints.org) | NOT PEER-REVIEWED | Posted: 10 August 2017 doi:10.20944/preprints201708.0037.v1

0.05 s, the sound wave is propagating but has not reached the soft boundary. Figure 10(c) and (d) is the sound pressure at t = 0.10 s and 0.15 s, respectively. A reflection sound wave is generated under the effect of the soft boundary, and the reflection sound wave propagates along the -x direction. The incident sound wave and reflection sound wave overlap with each other.

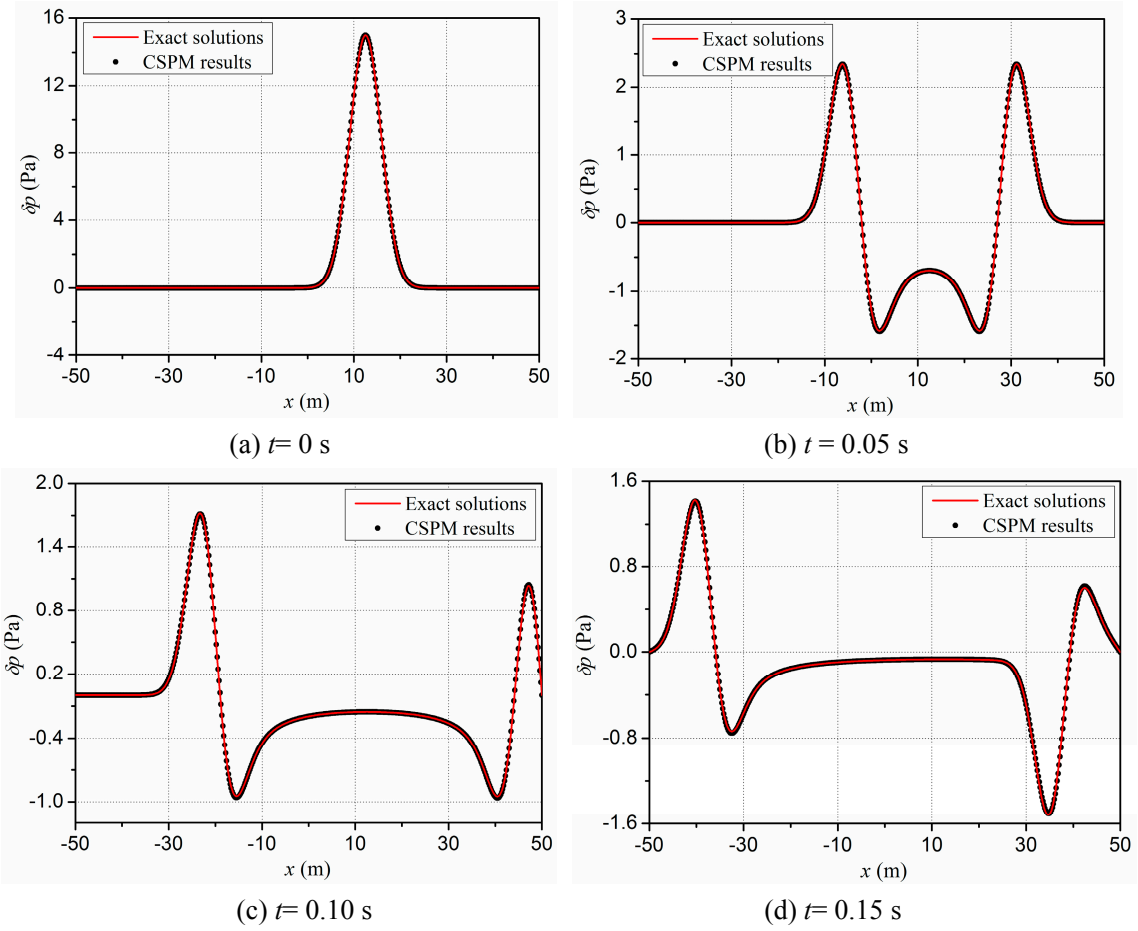

Figure 11. Sound pressure of particles at y = 0 m.

As shown in Figure 11, CSPM results are in good agreement with theoretical solutions, namely, the hybrid CSPM-FDTD method can accurately simulate the sound propagation with a soft boundary.

5.3 Rigid boundary

Sound reflection model with the rigid boundary is built. Simulation results are compared to theoretical solutions in Figure 12. Since the sound propagation process at t = 0.0 s and 0.05 s is the same as in Figure 10(a) and (b), Figure 12(a) and (b) just give the sound pressure of particles at t = 0.10 s and 0.15 s, respectively. Figure 13 shows sound pressure at y = 0 m.

Preprints (www.preprints.org) | NOT PEER-REVIEWED | Posted: 10 August 2017 doi:10.20944/preprints201708.0037.v1

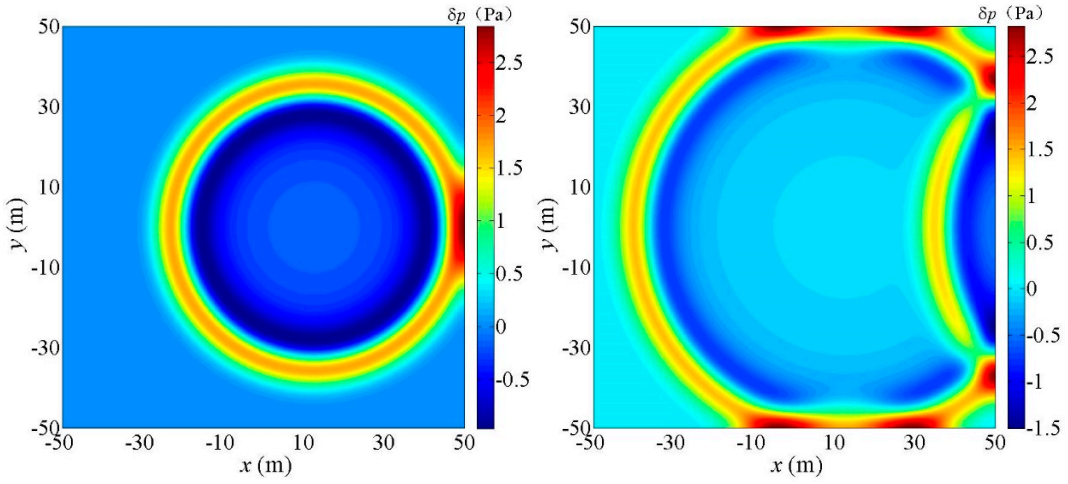

(a) t= 0.10 s (b) t= 0.15 s

Figure 12. The sound pressure contour of the Guassian pulse under the effect of rigid boundary.

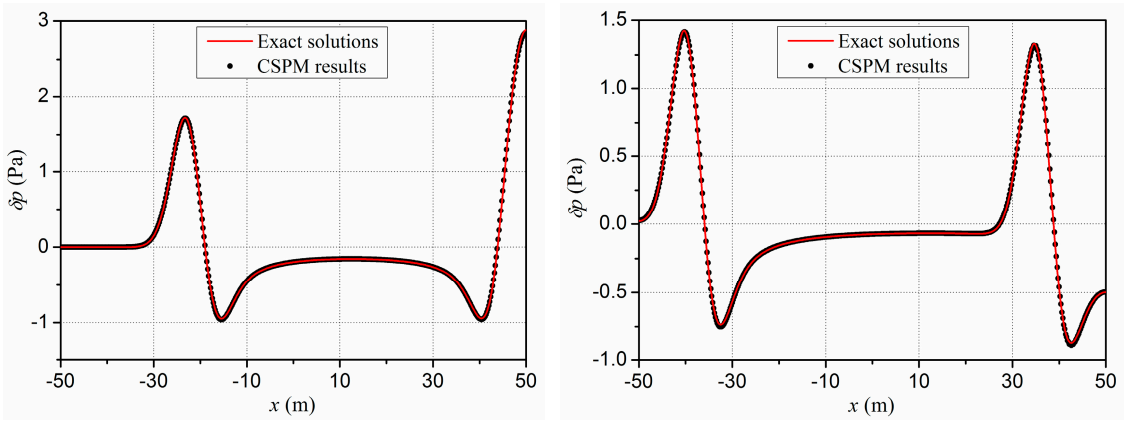

(a) t= 0.10 s (b) t= 0.15 s

Figure 13. The sound pressure of particles at y = 0 m.

It can be seen that the numerical simulation can handle the process of sound propagation and reflection correctly, even when the sound waves reach the boundary. The CSPM results give each peak of the sound waves almost the same as theoretical solutions.

5.4 Absorbing boundary

The sound propagation model with the implementation of absorbing boundary is built. Simulation results are shown in Figure 14 and Figure 15.

Preprints (www.preprints.org) | NOT PEER-REVIEWED | Posted: 10 August 2017 doi:10.20944/preprints201708.0037.v1

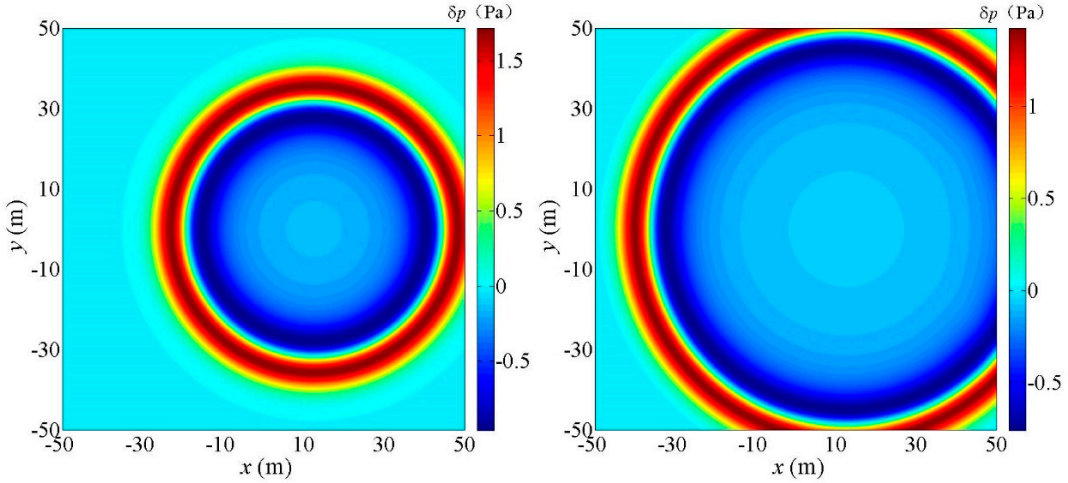

(a) t= 0.10 s (b) t= 0.15 s

Figure 14. The sound pressure contour of the Guassian pulse under the effect of absorbing boundary.

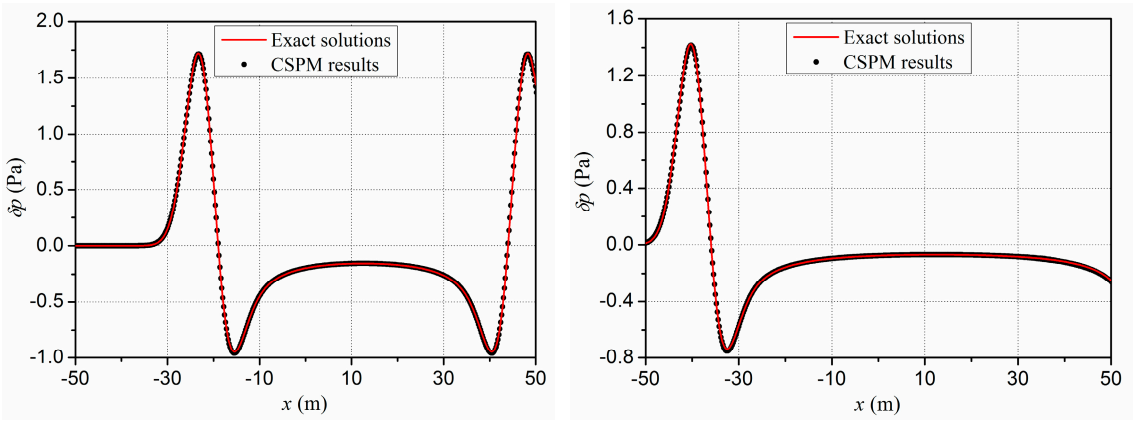

(a) t= 0.10 s (b) t= 0.15 s

Figure 15. The sound pressure of particles at y = 0 m.

Unlike soft and rigid boundary, under the effect of absorbing boundary, the incident wave cannot generate reflection wave. It can be seen from the figure, CSPM simulation results are in good agreement with theoretical solutions at each time. There is almost no reflecting sound pressure in the last figure. The absorbing boundary works well in the computation.

6. Sound Scattering

6.1 Computational model

A model is built for computing the sound scattering, as shown in Figure 16. This gives the geometry of the numerical model, where the object is a circular cylinder with a radius of r = 2 m, and the center is located at (x = 32 m, y = 32 m). A plane incident sound wave from the left, a Cartesian coordinate system is chosen in this model.

Since theoretical solutions exist for a circular cylinder with ideal boundary conditions, this sound scattering case is used to validate the CSPM algorithm with hybrid meshfree-FDTD boundaries. The

Preprints (www.preprints.org) | NOT PEER-REVIEWED | Posted: 10 August 2017 doi:10.20944/preprints201708.0037.v1

problem with infinitely rigid boundary is computed.

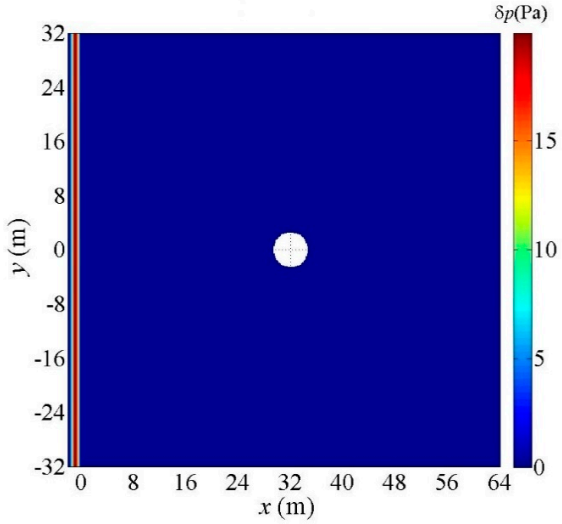

Figure16. The sound scattering model of cylinder.

The plane incident sound wave propagates from the region of $x < 0$ m to $x > 0$ m, the positive x-axis indicates the direction of the plane sound wave propagation. The computation domain is a rectangle area, and is located at $-2 \leqslant x \leqslant 64$ m, $-32 \leqslant y \leqslant 32$ m. The acoustic source of the plane wave is in the region of $-2 \leqslant x \leqslant 0$ m. when $t = 0$ s, the sound wave is located at $-2 \leqslant x \leqslant 0$ m, and sound pressure of the other region is zero.

The sound pressure of the plane sound wave in the region of $x < 0$ can be written as

$$\delta p\left(t, x<0\right) = P_{\mathrm{A}} - P_{\mathrm{A}} \cos\left(\omega t - kx\right) \tag{45}$$

where t represents the computation time, x is the geometrical position along the sound propagation direction. P_{A} is the amplitude of sound pressure, ω represents the angle frequency of plane wave, k is the wave number. The amplitude and angle frequency are set to 10 Pa and 1200 rad/s, respectively.

Table 2 lists the computation parameters that are used in CSPM-FDTD hybrid method for simulating the sound scattering.

Table 2. Parameters for the CSPMalgorithms of sound scattering.

Computational parameters	Values
Particle spacing Δx	0.10 m, 0.10 m
h	0.11 m
Kernel type	cubic spline
C_{CFL}	0.20
c_0	340 m/s
ρ_0	1.0 kg/m^3

6.2 Computational results

Basing on the cylinder model of sound scattering and computation parameters, the scattering of a

Preprints (www.preprints.org) | NOT PEER-REVIEWED | Posted: 10 August 2017 doi:10.20944/preprints201708.0037.v1

rigid cylinder with plane wave incidence is simulated, the rigid boundary is imposed on the cylinder, and the computation time is $t = 0.17$ s, the sound pressure contours of total field and scattered wave at different times are shown in Figure 17. Figures on the left side indicate the total sound pressure, while the figures on the right represent the sound pressure of scattered waves.

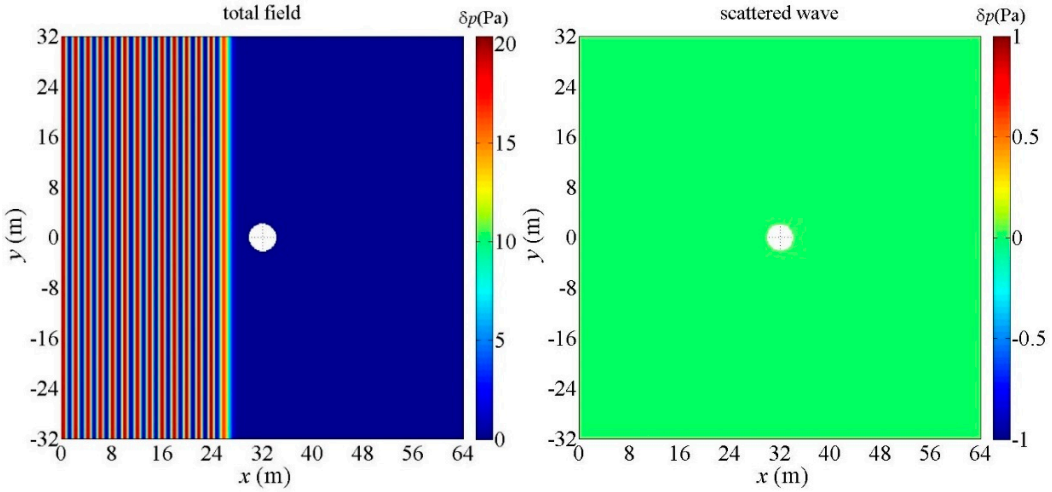

(a) $t = 0.08$ s

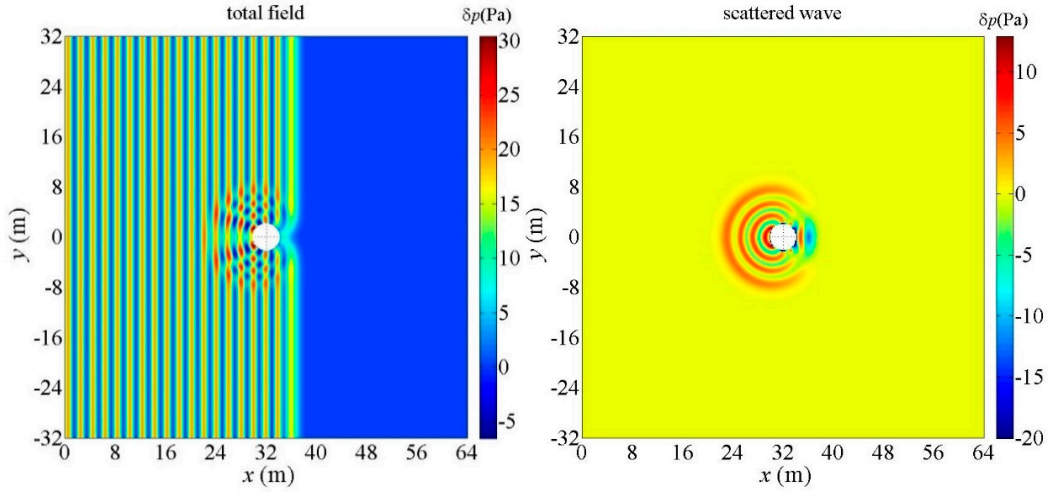

(b) $t = 0.11$ s

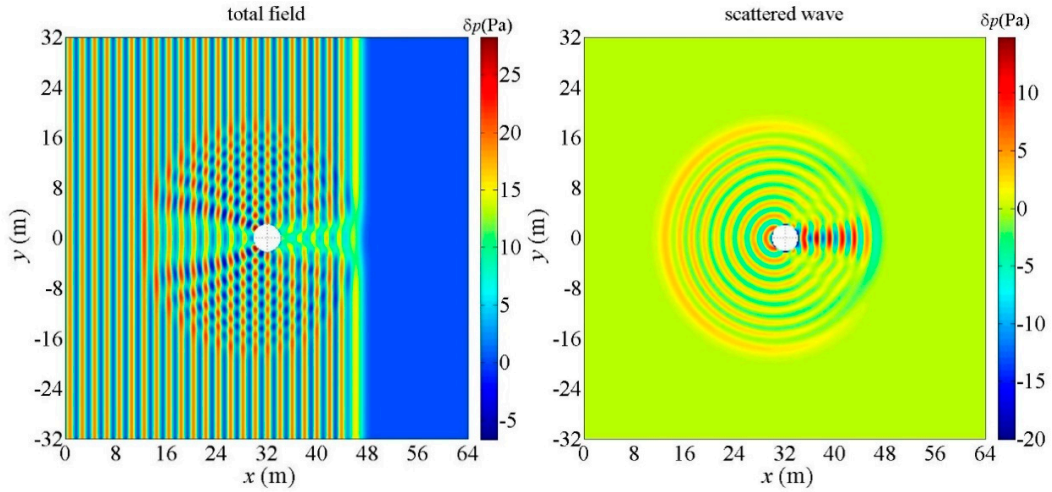

(c) $t = 0.14$ s

Preprints (www.preprints.org) | NOT PEER-REVIEWED | Posted: 10 August 2017 doi:10.20944/preprints201708.0037.v1

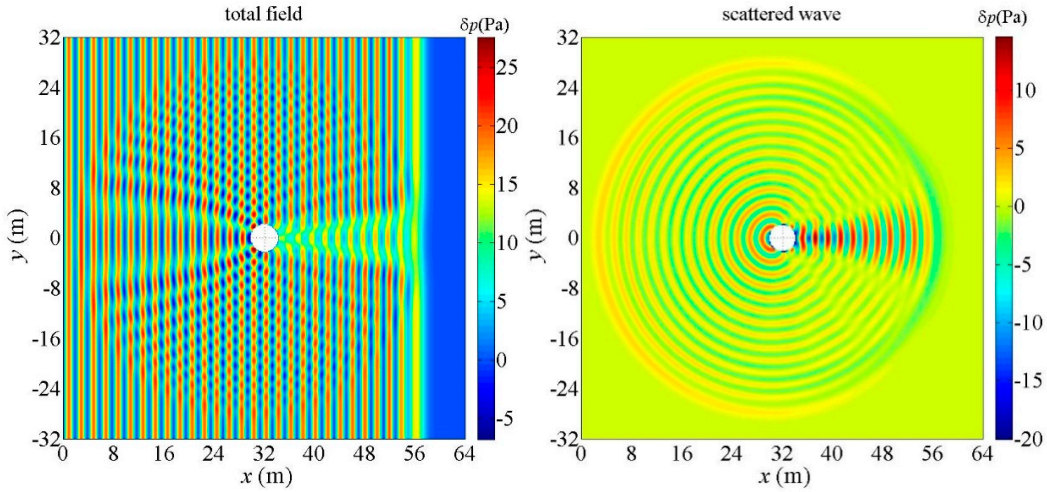

(d) t= 0.17 s

Figure 17. Sound pressure contour of scattering of rigid cylinder.

From the figure, it can be seen that the incident plane wave has not propagates to the cylinder, therefore, there is no scattered wave at t = 0.08 s. As time going, the incident plane wave propagates to the cylinder, and the scattered waves were emitted from the object, and interfered with the incident plane wave. In addition, the interfered region increases with the computation time.

In order to give a better view of the back scattering, patterns of sound pressure rather than intensity are presented. Figure 18 gives the far-field directional pattern of sound pressure amplitude. In this figure, the scattered points represent CSPM results, and the solid line is the exact solutions.

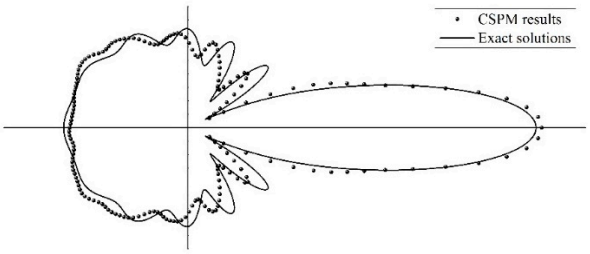

Figure 18. The directional pattern of sound scattering of rigid cylinder.

The scattering points is obtain by using the Fourier transform method from the near field, and a 180 points FFT are used in the computation. The figure indicates that the strongest scattering wave was in the forward direction. It is in the same phase with the incident wave, therefore adding the incident plane wave to yield a red region. In this region, the amplitude of sound pressure is bigger than the other region. The pattern is compared with the solid curve that represents a theoretical result. Good agreement between two curves provides a verification of the hybrid CSPM-FDTD algorithm.

7. Conclusions

The meshfree CSPM method is proposed to improve the accuracy in solving acoustic wave equations with particle-based acoustic methods. To represent different acoustic boundaries, a novel

 doi:10.20944/preprints201708.0037.v1

boundary treatment technique based on the hybrid meshfree-FDTD method is proposed. The treatments of soft, rigid, and absorbing boundary conditions are defined by using this hybrid method, and main computational parameters are discussed. The findings lead to following conclusions:

1. The CSPM method is effective for acoustic problems, and it has good convergence while maintaining a constant ratio of the particle spacing to the smoothing length.

2. A hybrid meshfree-FDTD method is developed and used as an acoustic boundary treatment technique for the meshfree method, and different boundaries are built for virtual particles by using this technique.

3. Sound wave propagation and how it is affected by an obstacle is simulated with soft, rigid, and absorbing boundaries. PCA results agree well with theoretical solutions in modeling benchmark problems in computational acoustics.

Acknowledgements: This study was supported by the Independent Innovation Foundation of Huazhong University of Science and Technology (No. 01-18-140019) and the Fundamental Research Funds for the Central Universities (WUT: 2017IVB081).

Conflict of Interests: The authors declare that there is no conflict of interests regarding the publication of this paper.

References

[1] Marburg S, Nolte B. *Computational acoustics of noise propagation in fluids: finite and boundary element methods*. New York, NY: Springer; USA, 2008.

[2] Kythe PK. *An Introduction to Boundary Element Methods*. CRC Press; 1995.

[3] Wang SZ. Finite-difference time-domain approach to underwater acoustic scattering problems. *J Acoust Soc Am* 1996; 99(4): 1924-1931.

[4] Lee D, McDaniel ST. *Ocean Acoustic Propagation by Finite Difference Methods*. Pergamon Press: Oxford; UK, 2014.

[5] Ihlenburg F. *Finite Element Analysis of Acoustic Scattering*. New York, NY: Springer; USA, 1998.

[6] Harari I. A survey of finite element methods for time harmonic acoustics. *Comput Methods Appl Mech Eng* 2006; 195(13–16): 1594-1607.

[7] Chai YB, Li W, Gong ZX, Li TY. Hybrid smoothed finite element method for two-dimensional underwater acoustic scattering problems. *Ocean Eng* 2016; 116: 129-141.

[8] Li W, Chai YB, Lei M, Li TY. Numerical investigation of the edge-based gradient smoothing technique for exterior Helmholtz equation in two dimensions. *Comput Struct* 2017; 182: 149-164.

[9] Godinho L, Amado-Mendes P, Carbajo J, Ramis-Soriano J. 3D numerical modelling of acoustic horns using the method of fundamental solutions. *Eng Anal Bound Elem* 2015; 51: 64-73.

[10] Fairweather G, Karageorghis A, Martin PA. The method of fundamental solutions for scattering and radiation problems. *Eng Anal Bound Elem* 2003; 27: 759-769.

[11] Uras RA, Chang CT, Chen Y, Liu WK. Multiresolution reproducing kernel particle methods in acoustics. *J Comput Acoust* 1997; 5: 71-94.

[12] Liu WK, Hao W, Chen Y, Jun S, Gosz J. Multiresolution reproducing kernel particle methods. *Comput Mech* 1997; 20(4): 295-309.

[13] Bouillard P, Suleau S. Element-free Galerkin solutions for Helmholtz problems: Formulation and numerical assessment of the pollution effect. *Comput Methods Appl Mech Eng* 1998; 162: 317-335.

[14] Belytschko T, Lu YY, Gu L. Element-free Galerkin methods. *Int J Numer Methods Eng* 1994; 37(2): 229-256.

[15] Lee S, Brentner KS, Morris PJ. Assessment of time-domain equivalent source method for acoustic scattering. *AIAA J* 2011; 49: 1897-1906.

[16] Lee S. Review: The use of equivalent source method in computational acoustics. *J Comput Acoust* 2016; 24: 1630001.

[17] Fu ZJ, Chen W, Gu Y. Burton-Miller-type singular boundary method for acoustic radiation and scattering. *J Sound Vib* 2014; 333: 3776-3793.

[18] Li J, Chen W, Fu Z. Numerical investigation on convergence rate of singular boundary method. *Math Prob Eng* 2016; 2016: 3564632.

[19] Tadeu A, Stanak P, Sladek J, Sladek V. Coupled BEM-MLPG acoustic analysis for non-homogeneous media. *Eng Anal Bound Elem* 2014; 44: 161-169.

[20] Leblanc A, Chardon G. Acoustic eigenanalysis of 2D open cavity with Vekua approximations and the method of particular solutions. *Eng Anal Bound Elem* 2014; 43: 30-36.

[21] Wolfe CT. *Acoustic modeling of reverberation using Smoothed Particle Hydrodynamics*. Master Thesis, University of Colorado; USA, 2007.

[22] Hahn P. *On the use of meshless methods in acoustic simulations*. Master Thesis, University of Wisconsin-Madison; USA, 2009.

[23] Zhang YO, Hou QZ, Gong ZX, Zhang T, Li TY, Wei JG, Dang JW. Lagrangian meshfree particle method for modeling acoustic wave propagation in moving fluid. The 173rd Meeting of the Acoustical Society of America, Boston, USA, 25-29 June, 2017.

[24] Zhang YO, Zhang T, Ouyang H, Li TY. Efficient SPH simulation of time-domain acoustic propagation. *Eng Anal Bound Elem* 2016; 62: 112-122.

[25] Zhang YO, Zhang T, Ouyang H, Li TY. Smoothed particle hydrodynamics simulation of sound reflection and transmission. *J Acoust Soc Am* 2014, 136: 2224.

[26] Zhang YO, Zhang T, Ouyang H, Li TY. SPH simulation of sound propagation and interference. In Proceedings of 5th International Conference of Computational Method (ICCM), Cambridge, UK, 28-30 July, 2014.

[27] Zhang YO. Solving time-dependent acoustic problems with a Lagrangian meshfree finite difference particle method. In Proceedings of 8th International Conference of Computational Method (ICCM), Guilin, China, 25-29 July, 2017.

[28] Zhang YO, Llewellyn Smith SG, Zhang T, Li TY. A Lagrangian approach for computational acoustics with meshfree method. Preprints 2017, 2017010115 (doi: 10.20944 / preprints 201701.0115.v1).

[29] Lucy LB. A numerical approach to the testing of the fission hypothesis. *Astron J* 1977; 82: 1013-1024.

[30] Gingold RA, Monaghan JJ. Smoothed Particle Hydrodynamics-theory and application to non-spherical stars. *Mon Not R Astron Soc* 1977; 181: 375-389.

[31] Liu MB, Liu GR. Smoothed Particle Hydrodynamics (SPH): an overview and recent developments. *Arch Comput Methods Eng* 2010; 17: 25-76.

[32] Liu MB, Liu GR, Zong Z. An overview on smoothed particle hydrodynamics. *Int J Comput Methods* 2008; 5: 135-188.

[33] Springel V. Smoothed particle hydrodynamics in astrophysics. *Annu Rev Astron Astrophys* 2010; 48: 391-430.

[34] Monaghan JJ. Smoothed particle hydrodynamics and its diverse applications. *Annu Rev Fluid Mech* 2012; 44: 323-346.

[35] Liu GR, Liu MB. Smoothed particle hydrodynamics: a meshfree particle method. World Scientific: Singapore, 2003.

[36] Zhang YO, Zhang T, Ouyang H, Li TY. SPH simulation of acoustic waves: effects of frequency, sound pressure, and particle spacing. *Math Prob Eng* 2015; 7: 348314.

[37] Chen JK, Beraun JE, Carney TC. A corrective smoothed particle method for boundary value problems in heat conduction. *Int J Numer Methods Eng* 1999; 46: 231-252.

[38] Chen JK, Beraun JE, Jih CJ. Completeness of corrective smoothed particle method for linear elastodynamics. *Comput Mech* 1999; 24: 273-285.

[39] Zhang GM, Batra RC. Modeified smoothed particle hydrodynamics method and its application to transient problems. *Comput Mech* 2004; 34: 137-146.

[40] Liu MB, Xie WP, Liu GR. Modeling incompressible flows using a finite particle method. *Appl Math Model* 2005; 29: 1252-1270.

[41] Zhang GM, Batra RC. Symmetric smoothed particle hydrodynamics (SSPH) method and its application to elastic problems. *Comput Mech* 2009; 43(3): 321-340.

[42] Batra RC, Zhang GM. SSPH basis functions for meshless methods, and comparison of solutions with strong and weak formulations. *Comput Mech* 2008; 41(4): 527-545.

[43] Dilts GA. Moving-Least-Squares-particle hydrodynamics. I: Consistency and stability. *Int J Numer Methods Eng* 1999; 44: 1115-1155.

 doi:10.20944/preprints201708.0037.v1

[44] Dilts GA. Moving least square particle hydrodynamics II: conservation and boundaries. *Int J Numer Methods Eng* 2000; 48: 1503-1524.

[45] Zhang YO, Li X, Zhang T. Modeling sound propagation using the corrective smoothed particle method with an acoustic boundary treatment technique. *Math Comput Appl* 2017; 22: 26.

[46] Monaghan JJ, Lattanzio JC. A refined particle method for astrophysical problems. *Astron Astrophys* 1985; 149: 135-143.

[47] Yee KS. Numerical solution of initial boundary value problems involving Maxwell's equations in isotropic media. *IEEE Trans Antennas Propag* 1966; 14: 302-307.

[48] Wang S. Finite-difference time-domain approach to underwater acoustic scattering problems. *J Acoust Soc Am* 1996; 99: 1924-1931.